



 Cite this: *RSC Adv.*, 2021, 11, 35093

Rational design of a selective and sensitive “turn-on” fluorescent probe for monitoring and imaging hydrogen peroxide in living cells†

 Jing Lu,^a Liang Ji^b and Yanyan Yu *^b

As one type of reactive oxygen species (ROS), hydrogen peroxide (H₂O₂) plays a key role in regulating a variety of cellular functions. Herein, a fluorescent probe N-Py-BO was well designed and synthesized and its ability for detecting H₂O₂ by fluorescence intensity was evaluated. In the design, the arylboronate ester group was acted as a reaction site for H₂O₂. Upon reaction with H₂O₂ under physiological conditions, the boronate moiety in the probe was oxidized, followed by detachment from the probe and as a result, a “turn-on” fluorescence response for H₂O₂ was acquired. Due to the D–A structure formation between *N,N'*-dimethylaminobenzene and the –CN group and the linkage by thiophene and C=C bonds to increase the conjugate length, this probe showed a remarkable red shift of emission wavelength (650 nm) as well as a large Stokes shift (214 nm). An excellent linear relation with concentrations of H₂O₂ ranging from 2.0 to 200 μM and a good selectivity over other biological species were obtained. Importantly, taking advantage of the low toxicity and good biocompatibility, the developed probe was successfully applied to monitoring and imaging H₂O₂ and its level fluctuation in living cells, which provided a powerful tool for evaluation of cellular oxidative stress and understanding the pathophysiological process of H₂O₂-related diseases.

Received 3rd September 2021

Accepted 16th October 2021

DOI: 10.1039/d1ra06620j

rsc.li/rsc-advances

1. Introduction

Hydrogen peroxide (H₂O₂), a stable molecule and a type of reactive oxygen species (ROS), is a major component in maintaining mitochondrial redox processes, and also serves as a messenger for mitochondrial damage.^{1–3} Cellular H₂O₂ is constantly produced with a steady-state concentration (~0.1 mM) to signal cell growth and proliferation, whereas higher levels of H₂O₂ (*e.g.* ~100 mM) trigger cell growth arrest or apoptosis.^{4–6} This imbalance induced by H₂O₂ overproduction can impair tissues and organ systems and then lead to aging, injuries, and diseases, such as malignant tumors, cardiovascular disease, Alzheimer's disease, Parkinson's disease, *etc.*^{7–10} For these reasons, quantitative analysis of H₂O₂ in biological content is key to understanding its multiple roles in redox signaling and oxidative stress.

Over the past decades, electrochemistry,^{11,12} mass spectrometry (MS),¹³ luminescence^{14–16} and fluorescence^{17–20} have been widely reported to detect intracellular H₂O₂. Among them,

fluorescence sensing method combined with confocal laser imaging technology has emerged as one of the most powerful and versatile tools for monitoring the localization, and transportation of vital biomolecules within the context of living systems.^{21–27} A number of well-designed fluorescent probes have been developed specifically for imaging H₂O₂.^{28–35} Most of these H₂O₂ probes are based on small molecule dyes, including traditional dichloro-dihydro-fluorescein diacetate (DCFH-DA) and selective probes, including boronate oxidation,^{36,37} Baeyer–Villiger reaction,^{38,39} and very recently Mislow–Evans rearrangement,⁴⁰ which are proved to be sensitive enough for H₂O₂ sensing.⁴ Among them, probes designed according to the boronate oxidation reaction have attracted extensive interest due to its high selectivity over other ROS.^{41,42} For example, In 2020, Hua's group has designed a NIR fluorescent probe employing reduced phenazine and *p*-boratebenzyl. Upon addition of H₂O₂, the *p*-boratebenzyl group was oxidized to *p*-hydroxy benzyl and then self-departed from the probe, thus turning on the fluorescence.³⁷ However, most these probes suffer from short emission wavelength or small Stokes shift, which result in poor signal-to noise ratios. It has been widely accepted that large Stokes shift is a key parameter to evaluate the performance of a fluorescent probe, which is quite important in biological imaging that can avoid self-quenching.⁴³ Commonly, the Stokes shift or emission wavelength can be feasibly regulated by modifying the molecular structure of

^aThe First Clinical Medical College, Xuzhou Medical University, 209 Tongshan Road, Xuzhou 221004, Jiangsu, China

^bJiangsu Key Laboratory of New Drug Research and Clinical Pharmacy, Xuzhou Medical University, 209 Tongshan Road, Xuzhou 221004, Jiangsu, China. E-mail: yyyxzmc@163.com; Tel: +86 516 83262138

† Electronic supplementary information (ESI) available: The MS, ¹H and ¹³C NMR spectra of the probe. See DOI: 10.1039/d1ra06620j



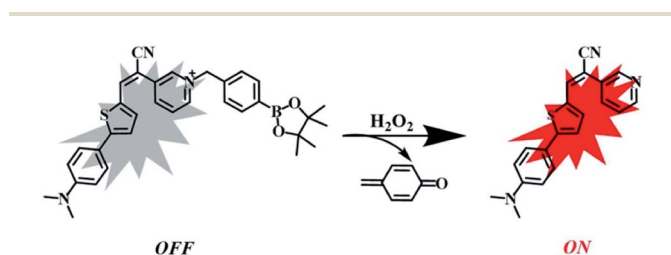
probe, such as construction of donor–acceptor (D–A) structure to effectively broaden absorption/emission wavelength.⁴⁴

Herein, in this work, a fluorescent probe named **N-Py-BO** was designed for H₂O₂ sensing and the chemical structure was displayed in Scheme 1. In this probe, the arylboronate ester group was acted as reaction site for H₂O₂ and as expected, the **N-Py-BO** probe showed high specificity for H₂O₂ over other reactive oxygen species (ROS), reactive nitrogen species (RNS) and biological species. Besides, a push–pull electronic architecture of D–A structure was formed between the electron-donating group of *N,N'*-dimethylaminobenzene and the electron-withdrawn groups of pyridine and –CN. This structure was linked by thiophene and C=C bond, which increased the conjugate length and led to the remarkable red shift of emission wavelength as well as a larger Stokes shift (214 nm). Reaction of **N-Py-BO** with H₂O₂ under physiological conditions caused the oxidation of the boronate moiety, followed by detachment from the probe and as a result, a “turn-on” fluorescent response was acquired, which led to the development of a highly sensitive and selective method for monitoring H₂O₂ in biological systems. Most notably, due to its low cytotoxicity and large Stokes shift, this probe has been successfully applied for the imaging of H₂O₂ and its level fluctuation in Raw 264.7 cells.

2. Experimental section

2.1 Materials and measurements

4-(Dimethylamino)phenylboronic acid and phorbol 12-myristate 13-acetate (PMA) were purchased from Macklin (Shanghai, China). 5-Bromothiophene-2-carbaldehyde and 4-bromomethylphenylboronic acid pinacol ester were obtained from energy-chemical (Shanghai, China). 3-Pyridineacetonitrile was bought from Bidepharmatech (Shanghai, China). H₂O₂ (30%) and *N*-acetyl-cysteine (NAC) were purchased from Aladdin (Shanghai, China). All other chemicals were used directly without further purification. All reactions were continuously stirred and monitored by thin layer chromatography (TLC). ¹H and ¹³C NMR spectra were taken on a JEOL 400 spectrometer. Mass spectra (MS) were measured on an America Agilent 1290/6550 mass spectrometer. Fluorescence spectra were recorded on an Agilent F-4600 fluorescence spectrophotometer. The fluorescent images were taken on a Leica STELLARIS 5 confocal laser scanning microscopy (CLSM).



Scheme 1 The possible response mechanism of the designed **N-Py-BO** probe toward H₂O₂.

2.2 Synthetic route of **N-Py-BO** probe

Synthesis of 5-(4-(dimethylamino)cyclohexa-1,5-dien-1-yl)thiophene-2-carbaldehyde (compound **1**). The compound **1** was synthesized by the established procedures from other group.⁴⁵

Synthesis of (*E*)-3-(5-(4-(dimethylamino)phenyl)thiophen-2-yl)-2-(pyridin-3-yl)acrylonitrile (N-Py**).** The compound **1** (231 mg, 1 mmol) and potassium hydroxide (84.17 mg, 1.5 mmol) were dissolved in ethanol (25 mL), and the mixture was stirred at room temperature. The reaction was monitored by TLC. And solid precipitation could be observed when the reaction was completed. The resultant product was then filtered, washed for several times using ethanol and purified by silica gel column chromatography (DCM : PE = 1 : 1) to obtain the compound **N-Py** (195.35 mg, 59%). ¹H NMR (400 MHz, CDCl₃) δ ppm: 8.90 (s, 1H, CH), 8.58 (d, *J* = 4.0 Hz, 1H, CH), 7.93 (d, *J* = 12.0 Hz, 1H, CH), 7.64–7.56 (m, 4H, Ar-H, 2 \times CH), 7.38–7.35 (m, 1H, Ar-H), 7.22 (d, *J* = 4.0 Hz, 1H, CH), 6.74 (d, *J* = 4.0 Hz, 2H, Ar-H), 3.03 (s, 6H, 2 \times CH₃). ¹³C NMR (100 MHz, CDCl₃) δ ppm: 152.19, 150.63, 148.86, 146.13, 145.14, 135.98, 134.49, 133.22, 127.44 (2C), 127.23, 123.85, 123.81, 121.42, 117.72, 112.45 (2C), 39.87 (2C). HRMS (ESI): calcd for C₂₀H₁₇N₃S [M + H]⁺ 332.1221; found: 332.1218.

Synthesis of (*E*)-3-(5-(4-(dimethylamino)phenyl)thiophen-2-yl)-2-(1-(4-(4,4,5,5-tetramethyl-1,3,2-dioxaborolan-2-yl)benzyl)-114-pyridin-3-yl)acrylonitrile (N-Py-BO**).** A mixture of **N-Py** (165.56 mg, 0.5 mmol) and 4-(bromomethyl)-benzeneboronic acid pinacol ester (220.59 mg, 0.75 mmol) in toluene was refluxed at 110 °C for 12 h. The obtained red powdery solid was filtered, washed with toluene and dried in vacuum to obtain the crude product. The crude product was further purified by silica gel column chromatography (DCM : MeOH = 16 : 1) to afford **N-Py-BO** (178.18 mg, 65%). ¹H NMR (400 MHz, DMSO-*d*₆) δ ppm: 9.60 (br, 1H, CH), 9.03 (d, *J* = 6.0 Hz, 1H, CH), 8.80 (d, *J* = 8.0 Hz, 1H, CH), 8.63 (s, 1H, CH), 8.23–8.19 (m, 1H, CH), 7.82 (d, *J* = 4.0 Hz, 1H, Ar-H), 7.75 (d, *J* = 8.0 Hz, 2H, 2 \times Ar-H) 7.64–7.57 (m, 5H, 5 \times Ar-H), 6.79 (d, *J* = 8.0 Hz, 2H, CH), 5.97 (s, 2H, CH₂), 3.00 (s, 6H, 2 \times CH₃), 1.29 (s, 12H, 4 \times CH₃). ¹³C NMR (100 MHz, DMSO-*d*₆) δ ppm: 154.03, 151.62, 143.47, 142.18, 141.52, 141.39, 140.44, 137.69, 135.79, 135.67 (2C), 133.54, 128.96, 128.81 (2C), 127.81 (2C), 122.76, 120.22, 117.57, 112.80 (2C), 97.04, 84.45 (2C), 64.05, 25.16 (4C). HRMS (ESI): calcd for C₃₃H₃₅BN₃O₂S [M]⁺ 548.2543; found: 548.2531.

2.3 Fluorescence measurements

A stock solution of 1 mM **N-Py-BO** probe was prepared in DMSO. Stock solutions of H₂O₂ (1 mM) and other analytes including Cys, GSH, Hcy, KI, MgCl₂, ZnCl₂, CuCl₂, NaHCO₃, H₂S, NaNO₂, NaNO₃, HClO, NaOH, were all prepared with deionized water. O₂^{•−} was produced from KO₂ stock solution in DMSO, which was prepared by adding KO₂ to DMSO (stored together with molecular sieve 4 Å) and sonicated the solution for 5 min. Singlet oxygen (¹O₂) was obtained by the reaction of NaClO (25 μ M) with H₂O₂ (25 μ M). Hydroxyl radicals ([•]OH) were generated in 200 μ M H₂O₂ catalyzed by 1 mM Fe²⁺. Peroxynitrite (ONOO[−]) was prepared by the reaction between 25 μ M NaNO₂ and 25 μ M

H₂O₂. For measurements, 10 μ L of the probe was taken out and incubated with different concentrations of H₂O₂ in 20 mM PBS buffer solution (pH = 7.4) containing 50% DMSO at room temperature for a certain time. The final concentration of the probe in the reaction system was 10 μ M. The fluorescence intensity was then measured with excitation wavelengths of 480 nm.

2.4 Cell culture and fluorescent imaging

Raw 264.7 and HeLa cells were both purchased from Gaining Biotechnology Co., Ltd (Shanghai, China). They were propagated in flasks cultured at 37 $^{\circ}$ C under a humidified 5% CO₂ atmosphere in DMEM medium, which were supplemented with 10% fetal bovine serum and 1% penicillin–streptomycin (10 000 U mL⁻¹ penicillin and 10 mg mL⁻¹ streptomycin). For cell imaging, Raw 264.7 cells were firstly seeded in glass-bottom culture dishes at a density of 1×10^5 cells per mL and cultured for 24 h. To demonstrate the capability of the designed N-Py-BO probe in tracking the variations of intracellular H₂O₂ levels under external stimulations, Raw 264.7 cells were pre-treated with culture medium containing 100 μ M H₂O₂, 1 μ g mL⁻¹ PMA (inducer of H₂O₂ production) alone or subsequent addition of 2 μ g mL⁻¹ N-acetyl-L-cysteine (NAC, an inhibitor of H₂O₂) for 2 h. The cells were then incubated with N-Py-BO for 30 min, followed by washing with saline solution for three times and the fluorescence images were observed under CLSM with excitation wavelengths of 488 nm.

2.5 Cytotoxicity assay

In this work, both of Raw 264.7 and HeLa cells were used to inspect the biocompatibility of the probe. Cells were seeded at a density of 1×10^4 per well in a 96-well plate for 24 h. Then, different concentrations of the probe (2, 4, 8, 12, 16 and 32 μ M) were added and incubated with cells for 48 h. After this, cell counting kit-8 solution (10% in DMEM medium) was added to each well and incubated for another 2 h. The absorbance at 450 nm was measured on a Thermo Fisher Microplate reader. Cell viability was calculated by the following equation: cell viability (%) = $((OD_{\text{treated}} - OD_{\text{blank}})/(OD_{\text{control}} - OD_{\text{blank}})) \times 100\%$.

3. Results and discussion

3.1 Design and synthesis of the probe N-Py-BO

The rationality of designing N-Py-BO probe was shown in Scheme 1. In order to synthesize a sensitive small molecule fluorescent probe for the detection of H₂O₂, this experiment used arylboronate ester group as H₂O₂-responsive unit shown in

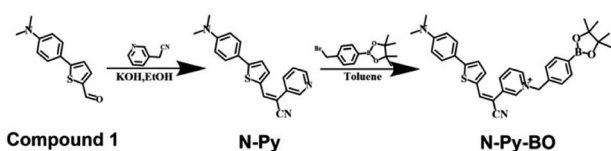


Fig. 1 Synthetic route of the N-Py-BO probe.

Fig. 1, which was reported to be able to recognize and respond to H₂O₂ under very mild conditions.³⁷ N,N'-dimethylaminobenzene could be acted as an electron-donating group to form a push–pull electronic architecture of D–A structure with pyridine group and –CN. Also, N,N'-dimethylaminobenzene and –CN group were linked by thiophene and C=C bond to increase the conjugate length, which led to the remarkable red shift of emission wavelength upon H₂O₂-mediated oxidation. H₂O₂ was capable of specifically recognize the arylboronate structure in N-Py-BO, which would fall off from the probe by H₂O₂ oxidization and form N-Py with D–A structure, so as to turn on the fluorescence.

The N-Py was synthesized according to reported literature,³⁷ followed by its reaction with 4-(bromomethyl)benzeneboronic acid pinacol ester to afford N-Py-BO. The chemical structure of N-Py-BO and N-Py were characterized by ¹H, ¹³C NMR and HRMS (Fig. S1–S6†). The synthetic route of this probe was shown in Fig. 1.

3.2 Fluorescent sensing of H₂O₂ by the designed N-Py-BO probe

Firstly, the absorption behavior of the N-Py-BO probe was studied. As shown in Fig. 2A, the N-Py (40 μ M) exhibited a maximum absorbance around 437 nm in PBS and DMSO mixed solution (v : v, 1 : 1, blue curve). After reacted with 4-(bromomethyl)benzeneboronic acid pinacol ester, the maximum absorption of the acquired N-Py-BO probe (40 μ M) red shifted to 498 nm (black curve). While after addition of 200 μ M H₂O₂, there was a blue shift of this peak to around 450 nm, which was close to that of N-Py (red curve). This change in the UV-vis absorption spectra before and after addition of H₂O₂ was likely to be the result of phenazine oxidation. According to the absorbance and emission spectrum in Fig. 2B, the Stokes shift was calculated to be 214 nm in this mixed medium for 10 μ M N-Py-BO probe. This large Stokes shift was beneficial to minimize the interferences caused by self-absorption effectively in confocal imaging.

For further verify the above results, the fluorescent sensing performance of the N-Py-BO probe toward H₂O₂ was also investigated in PBS and DMSO mixed solution. As observed from the fluorescent spectra in Fig. 3A, the probe (10 μ M) itself had no emission peak in the wavelength range from 550–

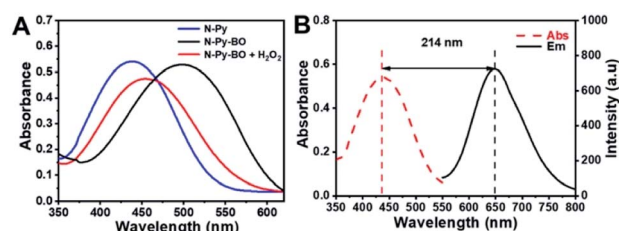


Fig. 2 (A) Absorbance intensity changes of N-Py (blue curve, 40 μ M) and N-Py-BO probe (40 μ M) in the absence (black curve) and presence of 200 μ M H₂O₂ (red curve) in PBS and DMSO mixed solution. (B) Absorbance and emission spectrum of the N-Py-BO probe in PBS/DMSO mixed solution.

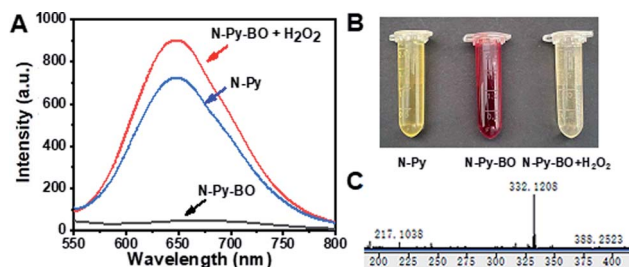


Fig. 3 (A) Fluorescence spectra of N-Py (10 μM), N-Py-BO probe (10 μM) alone or with addition of 200 μM H₂O₂ in PBS/DMSO mixed solution. (B) Colour changes of N-Py (50 μM) and N-Py-BO (50 μM) before and after reaction with 200 μM H₂O₂. (C) MS result obtained in N-Py-BO/H₂O₂ reaction system.

800 nm under excitation wavelengths of 480 nm. While after treated with 200 μM H₂O₂, a strong and obvious peak around 650 nm appeared. The H₂O₂-responsive emission peak around 650 nm was similar to that of N-Py. The fluorescence results were consistent with that of UV-vis in Fig. 2A, which jointly indicated that the change of fluorescence spectrum was a reflect of oxidation induced leaving of *p*-boratebenzyl as displayed in Scheme 1. It was noticed that during this reaction, the N-Py-BO probe presented an obvious color change from dark red to luminous yellow belonging to N-Py before and after treatment with H₂O₂ (Fig. 3B). In addition, the generation of N-Py after N-Py-BO reaction with H₂O₂ was also confirmed by MS, in which the peak of *m/z* 332.1208 (C₃₃H₃₅BN₃O₂S [M + H]⁺: 332.1221) was found in the MS spectrum of Fig. 3C. The above mechanism was further verified by HPLC experiments. As shown in Fig. S7,[†] the N-Py-BO probe showed an extensive peak at 9.58 min. After reaction with H₂O₂, a new peak appeared at 19.26 min, which shared the same retention time with that of N-Py. Combined with the above results, a “turn-on” fluorescent response was obtained, which led to the development of a sensitive method for monitoring H₂O₂ in abiotic systems.

3.3 Selectivity of N-Py-BO probe on H₂O₂

The selectivity of the probe on H₂O₂ monitoring was inspected. The probe was incubated with other reactive oxygen species (ROS), reactive nitrogen species (RNS) and reactive sulfur species (RSS) and the fluorescence intensity was determined in the same way as H₂O₂. As shown in Fig. 4, only the incubation with 200 μM H₂O₂ could induce the significant fluorescence enhancement of the probe, while under the same conditions, no fluorescence increase could be detected for other potential interferences, even at a much high concentration level (2.0 mM). Specifically, the response of H₂O₂ was 7.34-fold over ONOO⁻, and 18.26, 17.30, 14.69, 18.78, 16.75, 17.18, 19.05, 19.33, 17.07, 17.30, 16.75, 18.51, 19.47, 17.41, 13.62 and 15.28-fold over Cys, GSH, Hcy, K⁺, Mg²⁺, Zn²⁺, Cu²⁺, HCO₃⁻, H₂S, NO₂⁻, NO₃⁻, ClO⁻, OH⁻, O₂^{•-}, and ¹O₂ respectively. This result clearly suggested that the probe was highly selective for the discriminatory detection of H₂O₂, which provided an important basis for endogenous H₂O₂ imaging in living cells.

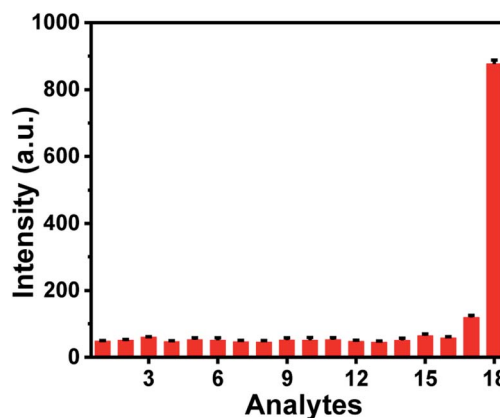


Fig. 4 Comparison of the fluorescence intensity of the N-Py-BO probe (10 μM) at 650 nm after incubated with 1–18: Cys, GSH, Hcy, K⁺, Mg²⁺, Zn²⁺, Cu²⁺, HCO₃⁻, H₂S, NO₂⁻, NO₃⁻, ClO⁻, OH⁻, O₂^{•-}, ¹O₂, ONOO⁻, and H₂O₂ (200 μM). Concentrations of the interferences were all 2.0 mM.

3.4 Optimizations, sensitivity and photostability

The response time of the probe toward H₂O₂ and concentrations of this probe were important parameters for the biological application of this probe and therefore were optimized. Firstly, the time-dependent fluorescence change of N-Py-BO probe was shown in Fig. 5A. The result indicated that the fluorescence intensity increased step-by-step when the reaction time was prolonged from 5 to 30 min and reached saturation at 30 min. The effect of probe concentration on the fluorescence intensity was also evaluated (Fig. 5B). Similarly, the fluorescence intensity was found increasing when the probe concentration ranged from 0 to 10 μM and there was no further increase after this point. Therefore, the optimal reaction time and probe concentration were set as 30 min and 10 μM throughout the whole experiment.

Under the optimal conditions, the titration test for H₂O₂ by this probe was carried out. As shown in Fig. 5C and D, the

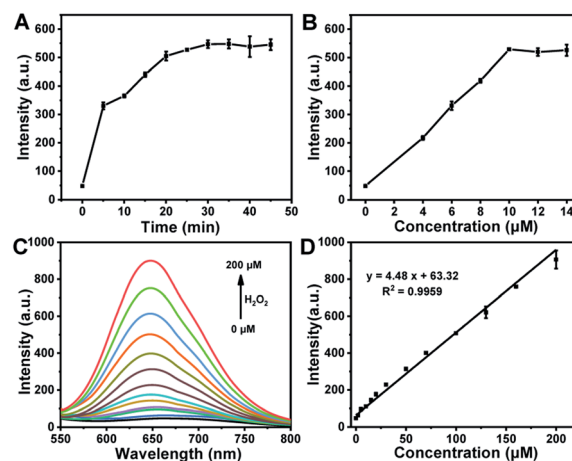


Fig. 5 (A) Time-dependent curve of the N-Py-BO probe (10 μM) at 650 nm toward 200 μM H₂O₂. (B) Effect of probe concentration on the fluorescence intensity. (C) The fluorescent spectrum of N-Py-BO probe with different concentrations of H₂O₂ from 0 to 200 μM . (D) The linear regression from fluorescence titration at 650 nm.

fluorescence intensity at 650 nm gradually increased along with increasing concentrations of H_2O_2 . A satisfactory linear relationship between the intensity and H_2O_2 concentrations in the range of 0–200 μM was acquired with the linear coefficient (R^2) of 0.9959. The detection limit was calculated to be about 0.57 μM at 3σ .

Finally, the photostability of the probe was tested within 7 days. As displayed in Fig. S8,† the probe itself showed a stable fluorescence intensity at 650 nm. Moreover, there was no significant difference for the responses toward 100 μM H_2O_2 between the first and the last day, indicating that the probe had a high photostability for H_2O_2 monitoring.

3.5 Cytotoxicity evaluations and confocal imaging of H_2O_2 in living cells

The cytotoxicity and biocompatibility of the probe was firstly evaluated by the conventional CCK-8 assay using Raw 264.7 and HeLa cells. As displayed in Fig. 6, upon exposure to the **N-Py-BO** probe with concentrations ranging from 2 to 32 μM , more than 85% of the two kind cells were viable under the experimental conditions, indicating that the designed probe was of low cytotoxicity to the cultured cells and possessed great potential for biological applications.

Then, the application of the probe for monitoring and imaging of H_2O_2 in living cells was assessed. As seen from Fig. 7, the tested Raw 264.7 cells treated only with 10 μM probe exhibited almost no fluorescence before treatment with any stimulant. After treatment of cells with 100 μM H_2O_2 for 2 h and subsequent with the probe for 30 min, a striking red fluorescence increase appeared, which was quite consistent with H_2O_2 -mediated boronate cleavage process occurred within these cells. The DAPI nucleus staining was employed herein to localize the cells, which exhibited blue fluorescence in the nucleus of cells. Meanwhile, the red signal of the probe was observed around cell cytoplasm. Moreover, the cell morphology under bright field further confirmed that the Raw 264.7 cells kept viable throughout the whole cell imaging experiments. Next, as PMA was a well-known kind of inducer for endogenous H_2O_2 generation through a cellular inflammation response,⁴¹ the fluctuation of H_2O_2 levels in Raw 264.7 cells after receiving PMA

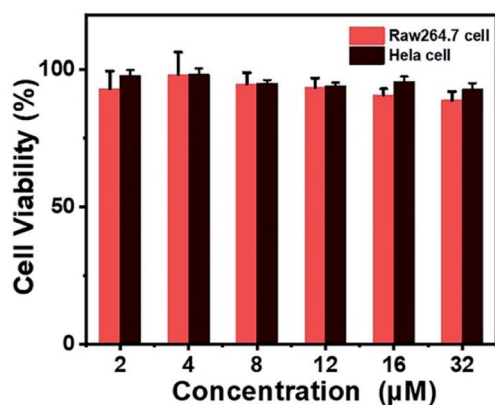


Fig. 6 Raw 264.7 and HeLa cell viabilities after incubated with different concentrations of **N-Py-BO** probe (2, 4, 8, 12, 16 and 32 μM) for 24 h.

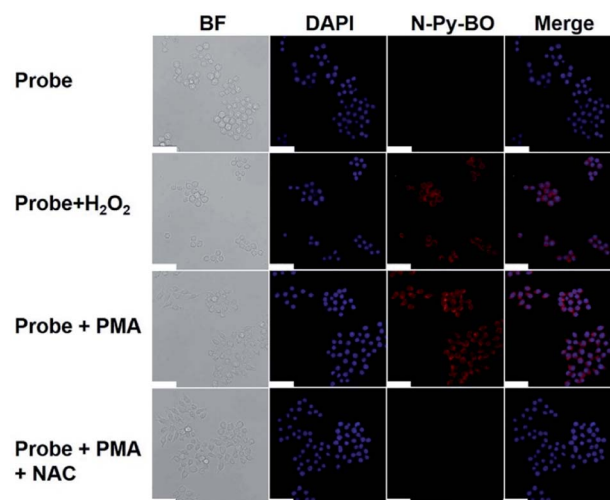


Fig. 7 Confocal images of RAW 264.7 macrophages incubated with **N-Py-BO** probe (10 μM) for 30 min or pretreated with 100 μM H_2O_2 , 1 $\mu\text{g mL}^{-1}$ PMA and 1 $\mu\text{g mL}^{-1}$ PMA + 2 $\mu\text{g mL}^{-1}$ NAC for 2 h and then the probe for 30 min. Scale bars represented 40 μm . Excitation wavelength: 488 nm.

stimulation was inspected by adding 1 $\mu\text{g mL}^{-1}$ PMA into cells. The images in Fig. 7 illustrated that the red fluorescence ascribed to the **N-Py-BO** probe became distinctly stronger, which was mainly caused by the production of large amount of H_2O_2 by this stimulation. In our next attempt, to verify that the increased signal was due to the endogenous H_2O_2 , rather than other species, NAC, an inhibitor of H_2O_2 generation, was further added afterwards PMA. As expected, there was nearly no detectable fluorescence after cells were firstly incubated with PMA and subsequent with NAC, suggesting that the increased fluorescence signal obtained in the PMA group was indeed resulted from H_2O_2 , not other biomolecular. The above cellular imaging results visually declared that the designed **N-Py-BO** probe was able to respond to exogenous and endogenous changes of H_2O_2 levels in living samples.

4. Conclusions

In summary, a new H_2O_2 fluorescent probe **N-Py-BO** was well designed and synthesized for the selective and sensitive monitoring of H_2O_2 . A rational design strategy by incorporating the specific reaction moiety with an extended conjugate structure was successfully implemented, producing a larger Stokes shift (214 nm) and a broadened emission wavelength. Notably, benefited from the low toxicity and good biocompatibility of the **N-Py-BO** probe, the exogenous and endogenous changes of H_2O_2 levels in living cells were able to be clearly and visually monitored and imaged. Overall, it can be expected that the designed probe holds a great potential for biomedical investigations on H_2O_2 -associated pathology and physiology.

Conflicts of interest

There are no conflicts to declare.

Author contributions

J. L. and Y. Y. designed the whole experiment. J. L. was responsible for the probe synthesis, fluorescence measurements and data analysis. L. J. performed the cellular experiments, including cell culture and imaging. Y. Y. completed the paper writing and editing.

Acknowledgements

We appreciated the financial supports from the National Natural Science Foundation of China (no. 21675137) and Natural Science Foundation of Jiangsu Province (BK20201457).

Notes and references

- 1 Z. Wu, M. M. Liu, Z. C. Liu and Y. Tian, *J. Am. Chem. Soc.*, 2020, **142**, 7532–7541.
- 2 M. Giorgio, M. Trinei, E. Migliaccio and P. G. Pelicci, *Nat. Rev. Mol. Cell Biol.*, 2007, **8**, 722–728.
- 3 H. Sies, *Redox Biol.*, 2017, **11**, 613–619.
- 4 S. Ye, J. J. Hu, Q. A. Zhao and D. Yang, *Chem. Sci.*, 2020, **11**, 11989–11997.
- 5 R. Kumar, J. Han, H.-J. Lim, W. X. Ren, J.-Y. Lim, J.-H. Kim and J. S. Kim, *J. Am. Chem. Soc.*, 2014, **136**, 17836G.
- 6 G. Filomeni, D. D. Zio and F. Cecconi, *Cell Death Differ.*, 2015, **22**, 377–388.
- 7 W. X. Wu, J. Li, L. Z. Chen, Z. Ma, W. Zhang, Z. Z. Liu, Y. N. Cheng, L. P. Du and M. Y. Li, *Anal. Chem.*, 2014, **86**, 9800–9806.
- 8 G. Y. Jiang, C. B. Li, X. Liu, Q. Q. Chen, X. K. Li, X. G. Gu, P. F. Zhang, Q. F. Lai and J. G. Wang, *Adv. Opt. Mater.*, 2020, **8**, 2001119.
- 9 W. Zhang, W. Liu, P. Li, F. Huang, H. Wang and B. Tang, *Anal. Chem.*, 2015, **87**, 9825–9828.
- 10 J. Liu, J. J. Liang, C. L. Wu and Y. B. Zhao, *Anal. Chem.*, 2019, **91**, 6902–6909.
- 11 T. Zhang, B. H. Zheng, L. Y. Li, J. J. Song, L. Song and M. D. Zhang, *Appl. Surf. Sci.*, 2021, **539**, 148255–148261.
- 12 S. Uzuncar, N. Ozdogan and M. Ak, *J. Electrochem. Soc.*, 2021, **168**, 076509–076523.
- 13 D. W. O'Sullivan, I. K. C. Silwal, A. S. McNeill, V. Treadaway and B. G. Heikes, *Int. J. Mass Spectrom.*, 2018, **424**, 16–26.
- 14 K. Motomiya, K. Sugita, M. Hagiwara and S. Fujihara, *ACS Omega*, 2019, **4**, 20353–20361.
- 15 L. Zhang, S. H. Yin, J. Z. Hou, W. P. Zhang, H. Huang, Y. X. Li and C. Yu, *Food Chem.*, 2019, **270**, 415–419.
- 16 D. F. Henning, P. Merkl, C. H. Yun, F. Lovino, L. Xie, E. Mouzourakis, C. Moularas, Y. Deligiannakis, B. Henriques-Normark and K. Leifer, *Biosens. Bioelectron.*, 2019, **132**, 286–293.
- 17 Q. Zhao, C. H. Zhou, Q. Y. Yang, Z. Y. Chu and N. Q. Jia, *Microchim. Acta*, 2019, **186**, 294–312.
- 18 Y. Y. Zuo, Y. Jiao, C. M. Ma and C. Y. Duan, *Molecules*, 2021, **26**, 3352–3364.
- 19 H. M. Zhong, S. R. Yu, B. Q. Li, K. D. He, D. Li, X. Wang and Y. X. Wu, *Chem. Commun.*, 2021, **57**, 6288–6291.
- 20 X. Y. Song, S. Bai, N. He, R. Wang, Y. L. Xing, C. J. Lv and F. B. Yu, *ACS Sens.*, 2021, **6**, 1228–1239.
- 21 Y. Ni, H. Liu, D. Dai, X. Q. Mu, J. Xu and S. J. Shao, *Anal. Chem.*, 2018, **90**, 10152–10158.
- 22 Y. Zhang, X. Q. Zhang, H. C. Yang, L. Yu, Y. J. Xu, A. Sharma, P. Yin, X. Y. Li, J. S. Kim and Y. Sun, *Chem. Soc. Rev.*, 2021, **50**, 11227–11248.
- 23 W. Tuo, Y. L. Xu, Y. F. Fan, J. Li, M. Q. Qiu, X. X. Xiong, X. Y. Li and Y. Sun, *Coord. Chem. Rev.*, 2021, **443**, 214017.
- 24 C. L. Li, C. Liu, Y. F. Fan, X. Ma, Y. B. Zhan, X. J. Lu and Y. Sun, *RSC Chem. Biol.*, 2021, **2**, 743–758.
- 25 P. Z. Wang, H. C. Yang, C. Liu, M. Q. Qiu, X. Ma, Z. Q. Mao, Y. Sun and Z. H. Liu, *Chin. Chem. Lett.*, 2021, **32**, 168–178.
- 26 W. J. Huang, H. C. Yang, Z. X. Hu, Y. F. Fan, X. F. Guan, W. Q. Feng, Z. H. Liu and Y. Sun, *Adv. Healthcare Mater.*, 2021, **10**, 2101003.
- 27 Y. L. Xu, Y. Zhang, J. Li, J. S. An, C. L. Li, S. Y. Bai, A. Sharma, G. Z. Deng, J. S. Kim and Y. Sun, *Biomaterials*, 2020, **259**, 120315.
- 28 J. Liu, J. J. Liang, C. L. Wu and Y. B. Zhao, *Anal. Chem.*, 2019, **91**, 6902–6909.
- 29 X. W. Wang, Y. Z. Huang, W. W. Lv, C. M. Lv, W. Zeng, Y. Zhang and X. P. Feng, *Anal. Methods*, 2017, **9**, 1872–1875.
- 30 Y. Xie, Z. Chen, L. N. Hu, H. L. Zhang, P. F. Xu and K. Pan, *Anal. Methods*, 2020, **12**, 1567–1569.
- 31 J. X. Huang, T. T. Li, R. N. Liu, R. Zhang, Q. Q. Wang, N. Li and Y. Q. Gu, *Sens. Actuators, B*, 2017, **248**, 257–264.
- 32 Y. C. Du, B. W. Wang, D. Jin, M. R. Li, Y. Li, X. L. Yan, X. Q. Zhou and L. G. Chen, *Anal. Chim. Acta*, 2020, **1103**, 174–182.
- 33 W. L. Jiang, W. X. Wang, J. Liu, Y. F. Li and C. Y. Li, *Sens. Actuators B-Chem.*, 2020, **313**, 128054.
- 34 W. X. Wang, W. L. Jiang, Y. Liu, Y. F. Li, J. Zhang and C. Y. Li, *Sens. Actuators B-Chem.*, 2020, **320**, 128296.
- 35 W. X. Wang, W. L. Jiang, G. J. Mao, M. Tan, J. J. Fei, Y. F. Li and C. Y. Li, *Anal. Chem.*, 2021, **93**, 3301–3307.
- 36 M. C. Chang, A. Pralle, E. Y. Isacoff and C. J. Chang, *J. Am. Chem. Soc.*, 2004, **126**, 15392–15393.
- 37 Y. C. Yan, L. Y. Liu, C. L. Li, Z. C. Yang, T. Yi and J. L. Hua, *Analyst*, 2020, **145**, 4196–4203.
- 38 M. Abo, Y. Urano, K. Hanaoka, T. Terai, T. Komatsu and T. Nagano, *J. Am. Chem. Soc.*, 2011, **133**, 10629–10637.
- 39 X. Xie, X. E. Yang, T. Wu, Y. Li, M. Li, Q. Tan, X. Wang and B. Tang, *Anal. Chem.*, 2016, **88**, 8019–8025.
- 40 D. Pham, U. Basu, I. Pohorilets, C. S. Croix, S. C. Watkins and K. Koide, *Angew. Chem., Int. Ed.*, 2020, **59**, 17435–17441.
- 41 L. Wu, A. C. Sedgwick, X. Sun, S. D. Bull, X. P. He and T. D. James, *Acc. Chem. Res.*, 2019, **52**, 2582–2597.
- 42 J. Ma, X. X. Wang, N. Li and Y. Cheng, *Sens. Actuators B-Chem.*, 2021, **346**, 130536–130544.
- 43 P. Verwilst, H. R. Kim, J. H. Seo, N. W. Sohn, S. Y. Cha, Y. Kim, S. Maeng, J. W. Shin, J. H. Kwak, C. Kang and J. S. Kim, *J. Am. Chem. Soc.*, 2017, **139**, 13393–13403.
- 44 W. X. Yao, Y. J. Cao, M. Y. She, Y. Y. Yan, J. X. Li, X. Leng, P. Liu, S. Y. Zhang and J. L. Li, *ACS Sens.*, 2021, **6**, 54–62.
- 45 W. Fu, C. X. Yan, Z. Q. Guo, J. J. Zhang, H. Y. Zhang, H. Tian and W. H. Zhu, *J. Am. Chem. Soc.*, 2019, **141**(7), 3171–3177.